Energy & Environmental Science

ROYAL SOCIETY OF CHEMISTRY

PAPER

View Article Online
View Journal | View Issue





Cite this: *Energy Environ. Sci.*, 2022, **15**, 1647

# Electrolyte design implications of ion-pairing in low-temperature Li metal batteries†

John Holoubek,[a] Kangwoon Kim,[b] Yijie Yin,[b] Zhaohui Wu,[c] Haodong Liu,[a] Mingqian Li,[c] Amanda Chen,[c] Hongpeng Gao,[b] Guorui Cai,[a] Tod A. Pascal,*[abcd] Ping Liu*[abcd] and Zheng Chen*[abcd]

Received 1st November 2021,
Accepted 3rd March 2022

DOI: 10.1039/d1ee03422g

rsc.li/ees

Lithium metal batteries are capable of pushing cell energy densities beyond what is currently achievable with commercial Li-ion cells and are the ideal technology for supplying power to electronic devices at low temperatures ($\leq -20$ °C). To minimize the thermal management requirements of these devices, batteries capable of both charging and discharging at these temperatures are highly desirable. Here, we report >4 V Li metal full cell batteries (N/P = 2) capable of hundreds of stable cycles down to −40 °C, unambiguously enabled by the introduction of cation/anion pairs in the electrolyte. *Via* controlled experimental and computational investigations in electrolytes employing 1,2-dimethoxyethane as the solvating solvent, we observed distinct performance transitions in low temperature electrochemical performance, coincident with a shift in the $Li^+$ binding environment. The performance advantages of heavily ion-paired electrolytes were found to apply to both the cathode and anode, providing Li metal Coulombic efficiencies of 98.9, 98.5, and 96.9% at −20, −40, and −60 °C, respectively, while improving the oxidative stability in support of >4 V cathodes. This work reveals a strong correlation between ion-pairing and low-temperature performance while providing a viable route to Li metal full batteries cycling under extreme conditions.

### Broader context

Electrochemical kinetics and their temperature dependence play a vital role in the performance and environmental operating limitations of high-energy batteries. Technologically, the kinetic limitations of standard cell chemistries preclude the cycling of Li metal batteries at sub-zero temperatures, which suffer a severe reduction in reversibility of plating and stripping and catastrophic shorting events due to dendritic growth. The limitations of secondary batteries in these temperature ranges have been proposed to be limited by the ion-desolvation penalty faced by $Li^+$ at the electrolyte/electrode interphase, for which few methods of optimization exist. In this work, we demonstrate the importance of ion-pairing between $Li^+$ and the anion within the electrolyte to low-temperature operation through a systematic study. In doing so, we demonstrate homogenous Li metal deposition, highly-reversible plating and stripping, and hundreds of stable cycles in >4 V Li metal full batteries down to −40 °C in an electrolyte system that would otherwise catastrophically fail under the same conditions without said ion-pairing in the solvation sphere. This work endeavors to unambiguously demonstrate the importance of solvation structure engineering in lithium battery electrolytes designed for operation under kinetic stress.

## Introduction

The advent of Li-ion batteries (LIBs) has enabled the rapid development of advanced portable electronics and electric vehicles. However, the application of existing and next-generation electronic devices in extremely low temperatures ($< -20$ °C) is currently limited by a significant reduction in the energy density of LIBs under such conditions.[1–5] Li metal batteries (LMBs), which replace the graphite anode (372 mA h $g^{-1}$) with Li metal (3860 mA h $g^{-1}$), have gathered recent interest to improve cell-level energy density, and if realized would be the ideal technology for low-temperature devices.[6] However, LMBs are known to face poor cycling stability due to the inherent reactivity and volume change of the Li metal anode. These factors present as a low Coulombic efficiency (CE) during repeated plating and stripping and may result in dendritic Li growth which may penetrate the battery separator and short the cell.[7,8] What's more, cycling of the Li metal anode

[a] *Department of NanoEngineering, University of California, San Diego, La Jolla, CA 92093, USA. E-mail: tpascal@eng.ucsd.edu, piliu@eng.ucsd.edu, zhengchen@eng.ucsd.edu*
[b] *Program of Materials Science and Engineering, University of California, San Diego, La Jolla, CA 92093, USA*
[c] *Program of Chemical Engineering, University of California, San Diego, La Jolla, CA 92093, USA*
[d] *Sustainable Power and Energy Center, University of California, San Diego, La Jolla, CA 92093, USA*

† Electronic supplementary information (ESI) available. See DOI: 10.1039/d1ee03422g

under sub-zero conditions further exacerbate these effects.[9–11] To overcome these challenges, significant advancements in battery engineering and a scientific understanding of these devices and their temperature scaling is crucial.

To address the capacity and voltage loss experienced by secondary batteries at low temperature, engineering of the electrolyte chemistry has emerged as a promising tool.[8–16] Though there has been much progress in the improvement of low temperature battery performance, most works have focused on the improvement of low temperature discharge following a charge at benign temperatures.[2,4,15,16] Unless the device employing such batteries can be removed from the cold operating environment during charge, this operation protocol inherently couples the designed battery to an external warming device. These warming systems consume non-negligible power and contribute mass to the overall system, thus reducing overall operating efficiency and energy density.[17,18] For applications that must be charged in their working environment, enabling low temperature charge and discharge is necessary to reduce or eliminate the need for thermal management at low temperature. For LMBs, this implies that Li metal must be reversibly plated and stripped under these conditions.

Along with technological progress, a more rigorous understanding of the interplay between various limiting factors at low temperature is necessary. Historically, improving the bulk ionic conductivity, solid–electrolyte interphase (SEI) composition, and $Li^+$ charge-transfer penalty have been the foremost goals of low temperature electrolyte design.[3,4,9–11,19–21] Among these factors, it has been suggested that the charge-transfer penalty is the dominant limitation among systems with sufficient bulk transport.[2,22,23] However, the heterogenous charge-transfer process in electrochemical systems is invariably complicated, particularly given that there is no mechanistic consensus regarding $Li^+$ dynamics at the electrode interphase in the presence of a SEI. While it is clear that factors such as SEI composition, $Li^+$ solvation structure, and interphasial dynamics play important roles in this process, their influence on one another is largely unknown. Hence, the technological advancement of temperature-resilient energy storage is heavily linked to a fundamental understanding of the charge-transfer process.

Our previous work aimed to provide low temperature system design principles based on the hypothesis that the solvation environment of the $Li^+$ ion in the electrolyte defines the charge-transfer barrier and its temperature dependence.[23] While we demonstrated state-of-the art Li metal reversibility down to −60 °C, the design insights gleaned from the LMB electrolyte of interest raised many questions that have yet to be answered. It was concluded that solvents of weak $Li^+$ binding were crucial to advantageous temperature scaling of Li metal reversibility, which agrees with the results from Li *et al.*,[22] Fan *et al.*,[16] and Wang *et al.*[24] However, such weak binding solvents commonly result in $Li^+$/anion binding in bulk solution, making a direct correlation between low temperature performance and any one factor difficult. This work aims to decouple the influence of ion-pairing and $Li^+$/solvent binding energy to gain a more definitive sub-zero LMB electrolyte design rationale and provide further insights on the temperature dependence of charge-transfer.

To provide such data, we propose a detailed comparison of electrolytes composed of the same solvating solvent with varying degrees of ion-pairing. The most direct way to accomplish this would be varying the solvating solvent/Li salt ratio.[25–27] However, the high viscosity of such electrolytes make this untenable when scaling to low temperatures, where any advantage in interphasial charge-transfer kinetics would be completely obscured by the overwhelming decrease in ionic conductivity.[16] Fortunately, a solution to this already exists in the advent of localized high-concentration electrolytes (LHCEs). These systems apply diluent solvents, which interact weakly with $Li^+$ and dissolve negligible salt on their own, in order to reduce the bulk viscosity of high-concentration electrolytes.[28–30] In doing so, any effects of ion-pairing in the $Li^+$ solvation shell can be decoupled from the bulk ionic conductivity of the solution at low temperature. LHCEs employing 1,2-dimethoxyethane (DME) was chosen as the primary basis of this investigation. This solvent has been well established to provide reversible room temperature Li metal performance when paired with lithium bis(fluoro sulfonyl)imide (LiFSI), even at dilute concentrations. However, the temperature dependence of Li reversibility is demonstrably acute,[23,31,32] which we and others have proposed to be linked to its strong binding with $Li^+$. Thus we pair the LiFSI/DME components with a bis(2,2,2 trifluoro ethyl)ether (BTFE) diluent, which allows for the modulation of the degree of ion-pairing while maintaining a relatively low bulk viscosity. We incrementally alter the BTFE/DME volume ratio from 1 M LiFSI in pure DME to 1 M LiFSI BTFE/DME (7 : 1, 8 M equivalent local concentration). Using both theoretical and experimental methods, we demonstrate that there is a distinct ion-pairing transition when the local concentration exceeds 4 M (3 : 1 BTFE/DME ratio), which results in vastly improved Li metal performance at low temperatures, while improving the oxidative stability and thus enabling the implementation of $LiNi_{0.8}Mn_{0.1}Co_{0.1}O_2$ (NMC 811) as a cathode material. This concept was utilized to design LMBs capable of charging and discharging at low temperatures, as illustrated in Fig. 1.

To provide a basis for the assessment of low temperature Li metal performance and the eventual design of LMB full batteries, physical characterization of the DME-based electrolytes of interest was first conducted. Though our previous results have indicated exceptional ionic conductivity is not necessarily a prerequisite for reversible low temperature Li metal performance,[23] the freezing of electrolytes and exponential increases in their viscosity is known to overwhelm electrochemical performance.[11,21] As shown in Fig. 2a, it was confirmed that all systems of interest remained in a liquid state down to −60 °C. To provide an insight into the effect of temperature on ionic transport, the ionic conductivities were also measured (Fig. 2b). It was found that the systems of lowest local concentration (*i.e.*, lowest DME/LiFSI ratio but still 1 M with respect to the total volume of BTFE and DME) displayed far superior transport, where the 1 M LiFSI in DME, 1 : 1, 3 : 1, 5 : 1, and 7 : 1

 

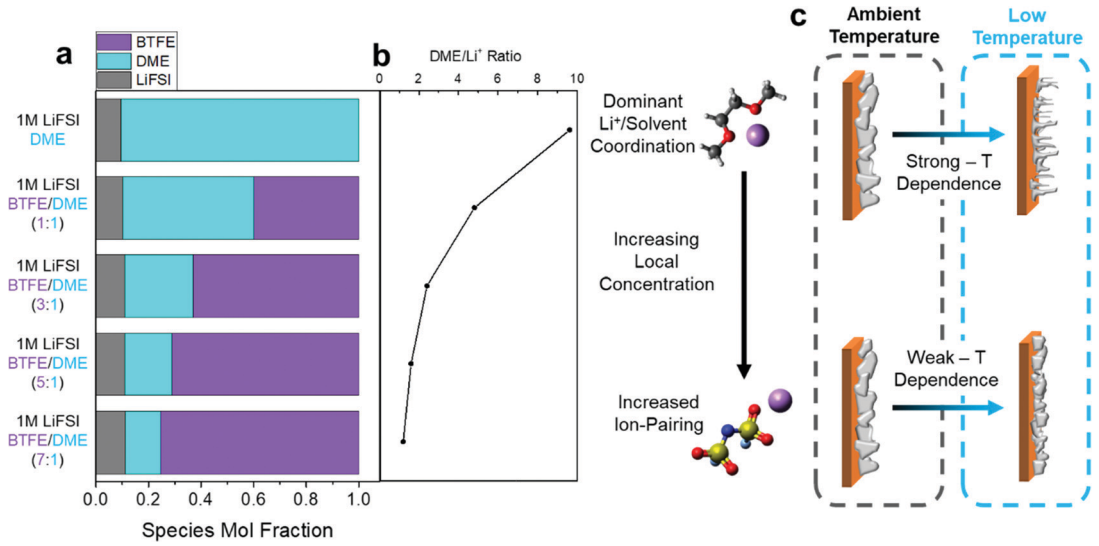


Fig. 1 Overview of (a) electrolytes of interest and their molar composition, (b) coincident effect of molar DME/$Li^+$ ratio on ion-pairing in solution, and (c) the effect of these factors on the temperature dependence of Li cycling.

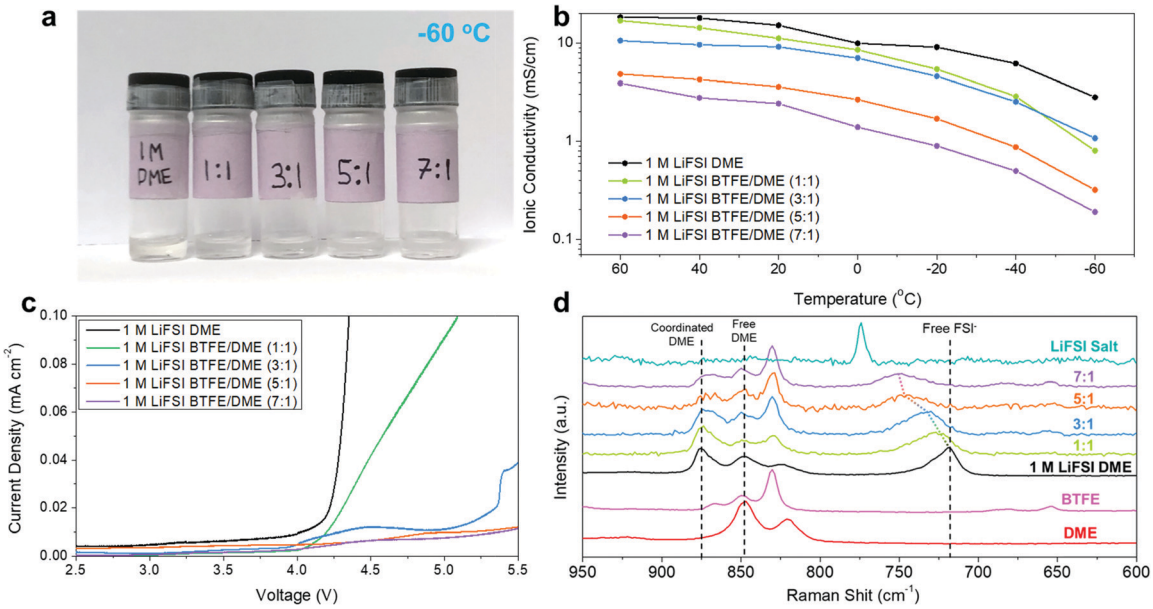


Fig. 2 Physical and electrochemical properties of the electrolytes of interest. (a) Optical photograph of electrolytes at −60 °C. (b) Measured ionic conductivity across temperature. (c) Oxidative linear scan voltammetry of selected systems on Al current collectors at 1 mV $s^{-1}$. (d) Raman spectra of the electrolytes and their pure components.

BTFE/DME electrolytes displayed ionic conductivities of 15.2, 11.2, 9.18, 3.60, and 2.43 mS $cm^{-1}$ at 20 °C, respectively. This trend was largely maintained at low temperature, where the systems retained 6.20, 2.87, 2.54, 0.87, and 0.50 mS $cm^{-1}$ at −40 °C, respectively. The reduction of bulk conductivity with increased ion-pairing is well-established, and can be generally described by a reduction in ionicity due to the strong interactions between cation and anion.[28,33] It is also noteworthy that the inclusion of BTFE in the electrolytes were found to slightly increase the viscosity, where the 1 M LiFSI DME, 1 M LiFSI BTFE/DME (1 : 1) and 1 M LiFSI BTFE/DME (5 : 1) electrolytes displayed viscosities of 1.7, 2.7, and 2.4 cP, respectively, however the viscosity of these systems all remains below that of conventional carbonate systems (Fig. S1, ESI†). Although ion-pairing is hypothesized to result in improved charge-transfer kinetics, its tradeoff with bulk transport may indicate that an intermediate concentration may be optimal for low-temperature LMB applications.

Electrolytes utilizing DME generally display poor oxidative stability due to the inherent HOMO energy of ether solvents.[29,34,35]

Though these systems are typically applied in Li–S batteries, the low-temperature performance degradation of the S cathode has been observed to be severe, due in large part to clustering processes inherent to the polysulfide conversion process.[1] As such, transition metal oxide cathode hosts remain to be highly desirable for low temperature applications, which require the oxidative stability of the electrolyte to exceed 4 V *vs.* $Li/Li^+$. Despite its disadvantages for ion transport through the bulk, increased local concentration (and increased ion-pairing) is known to produce advantageous effects on the electrochemical stability of the system.[25–29] This was found to be the case for the DME-based LHCE systems investigated here as well, where the areal current produced by linear-scan voltammetry (LSV) on an Al current collector was found to exceed 0.02 mA $cm^{-2}$ at 4.22, 4.31, 5.34, > 5.5, and >5.5 V for 1 M LiFSI in DME, 1 : 1, 3 : 1, 5 : 1, and 7 : 1 BTFE/DME, respectively (Fig. 2c). However, it is worth noting that there is a slight increase in oxidative current between 3.7 and 4.5 V within the 3 : 1 LSV profile, which indicates that a slight decomposition reaction occurs to form a passivating interphase, after which the current decreases again. It was also found that these trends were maintained in the presence of conductive carbon and NMC 811, where 1 M LiFSI DME and 1 M LiFSI BTFE/DME (1 : 1) showed significantly increased decomposition behavior at lower voltages than their counterparts (Fig. S2, ESI†).

The transport and electrochemical stability trends are a direct symptom of increased ion-pairing due to heightened local concentrations (*i.e.*, lower DME/$Li^+$ ratio). To observe this experimentally and to serve as an aid to future computational studies, Raman spectroscopy was carried out on the electrolytes of interest and their pure components (Fig. 2d). It was found that the S–N–S bending peak of the $FSI^-$, present in the salt spectra at 774 $cm^{-1}$, undergoes a significant shift to 719 $cm^{-1}$ when dissolved at 1 M in DME, indicative of the separation between $Li^+$ and $FSI^-$ produced by the DME. This peak was then found to progressively shift to 732 $cm^{-1}$ in the 3 : 1 mixture, which indicates an increase in ion-paring between $Li^+$ and $FSI^-$ in solution.[28] Though the peak shift between 1 M LiFSI DME and 1 M LiFSI BTFE/DME (3 : 1) appears to be linear, it is noteworthy that this shift is substantially heightened between the 3 : 1 and 5 : 1 systems. Additionally, the 5 : 1 and 7 : 1 mixtures display much broader S–N–S peaks, indicating an increased amount of bound $FSI^-$ solvation states within the system. Moreover, a similarly large reduction in conductivity was observed between the 3 : 1 and 5 : 1 mixtures (Fig. 2b). This ion-pairing was also found to result in a slight but incremental increase in $Li^+$ transference number, from 0.32 in 1 M LiFSI DME to 0.53 in the 7 : 1 system (Fig. S3, ESI†). Though this increase is significant, our previous work indicates that such an increase has little effect on the interphasial $Li^+$ depletion when observed in tandem with a reduction of ionic conductivity of such a magnitude.[23] These phenomena are further examined in the molecular dynamics analysis below.

To examine the implications of these electrolyte properties on low-temperature LMB reversibility, the CE of Li plating was determined in Li||Cu cells *via* the accurate galvanostatic method proposed by Adams *et al.*[36] Testing at 23 and −20 °C was conducted at 0.5 mA $cm^{-2}$ whereas we used 0.25 mA $cm^{-2}$ for −40 and −60 °C. Due to the intrinsic reductive stability of ether solvents and the fluorine-donating capabilities of LiFSI, 1 M LiFSI DME, and 1 M LiFSI 1 : 1, 3 : 1, 5 : 1, and 7 : 1 BTFE/DME systems were found to display reversible CEs of 96.0, 99.1, 99.1, 99.4, and 99.4% at room temperature (Fig. 3a). These CEs were also found to persist over many plating and stripping cycles (Fig. S4, ESI†). The relatively improved CEs of the electrolytes containing BTFE is likely due to the increased prevalence of fluorine in the SEI layers, which was confirmed *via* XPS (Fig. S5, ESI†), however the chemical identity of the SEI was found to be relatively similar across systems, which agrees with previous literature.[37] However, when the temperature was reduced it was found that the scaling of such reversibility was not equal across the systems. In particular, systems of lower local concentration displayed substantial noise in the voltage curves, which can be attributed to soft-shorting events at low temperature and contribute to extremely reduced CEs.[9,23] Specifically, the 1 M LiFSI DME electrolyte was found to short at −20 °C, whereas the CE of the 1 : 1 mixture reduced to 94.8% at −20 °C (Fig. 3b), before finally shorting at −40 °C. At −40 and −60 °C, the 3 : 1, 5 : 1, and 7 : 1 electrolytes were found to produce reversible CEs of 98.9, 98.5, 98.6, and 96.6, 96.9, 96.4%, respectively (Fig. 3c and d). A summary of these trends is shown in Fig. 3e for ease of comparison.

Additionally, the critical current for each electrolyte was assessed in Li||Li cells at each temperature. The profiles for these tests are shown in Fig. S6 (ESI†), where it was found that the 1 M LiFSI BTFE/DME (5 : 1) electrolyte maintains critical currents of 5, 3, and 0.75 mA $cm^{-2}$ at −20, −40, and −60 °C, which is the highest among the investigated systems. It is also worth noting that the critical current often exceeds the shorting currents observed in Li||Cu tests, which implies that nucleation of Li on Cu also plays a role in the poor performance. Indeed, previous reports have observed a substantial variance in nucleation behavior at reduced temperatures.[31] A summary of these critical currents is shown in Fig. 2f, which provides a basis for safety assessment at the full cell level. Crucially, we note that the optimal electrolytes for low temperature Li metal performance and ionic conductivity do not align, which agrees with previous reports and indicates that the low temperature performance is dictated by charge-transfer.[22,23]

To further understand the interplay between ion-pairing and Li metal performance at low temperature from a morphological standpoint, scanning electron microscopy (SEM) was conducted on Li deposited on Cu current collectors at 23 and −40 °C. Photographs taken of the Cu electrodes after deposition at 23 °C reveal metallic Li deposits with a silver appearance, which is typically indicative of micron-scale Li deposits, as uncontrolled nanoscale morphologies typically appear black in color (Fig. 4a). SEM images of the Li deposited at room temperature confirm this, where Li was found to deposit in the ''chunk'' morphology often associated with electrolytes of similar composition.[28–30,37] Interestingly, the micro-scale uniformity was found to increase coincidently with increasing local

 

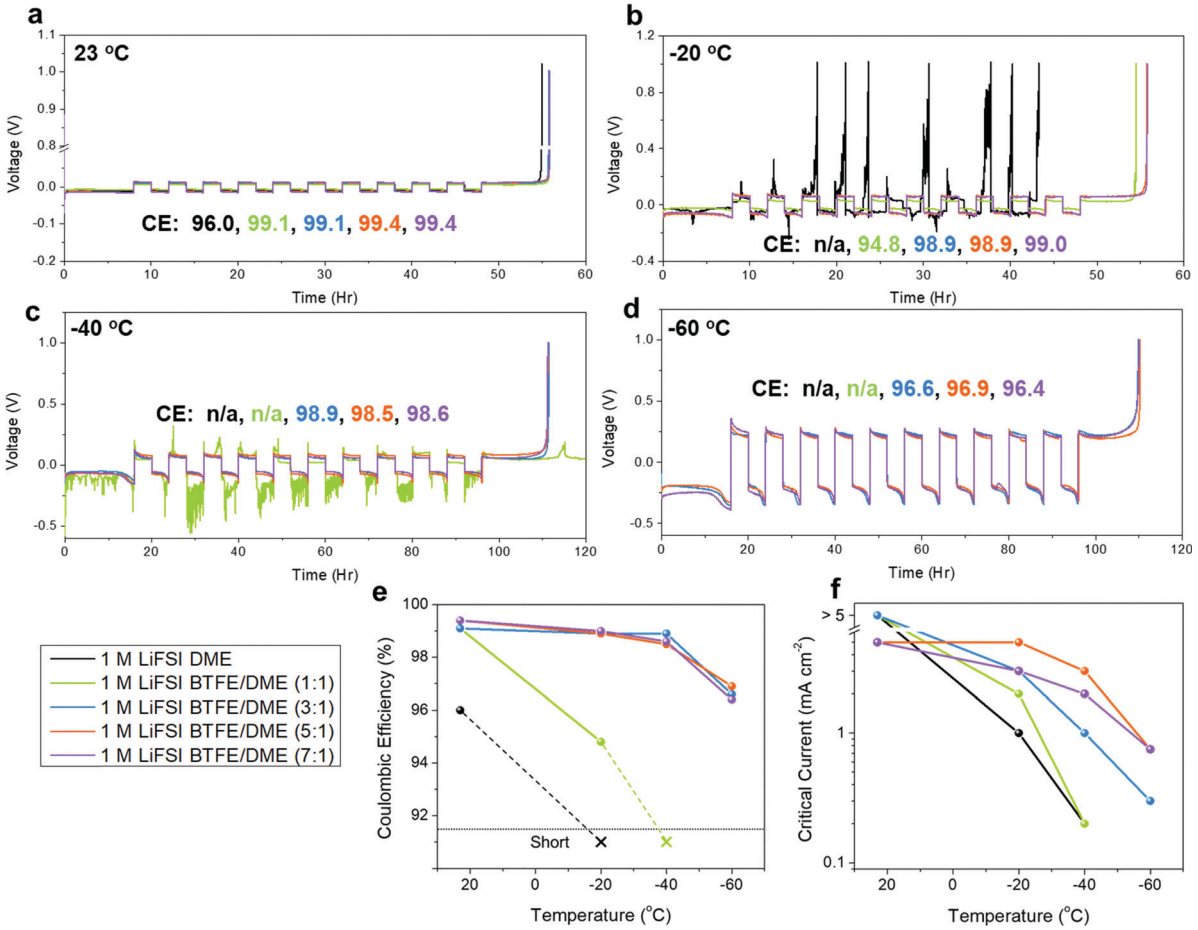


Fig. 3 Li metal performance measurements at room and low temperature. Voltage profiles of Li/Cu cells employing electrolytes of interest at (a) 23 °C and 0.5 mA $cm^{-2}$, (b) −20 °C and 0.5 mA $cm^{-2}$, (c) −40 °C and 0.25 mA $cm^{-2}$, (d) −60 °C and 0.25 mA $cm^{-2}$. In all cases a conditioning cycle was conducted and not shown. Summaries of (e) coulombic efficiency and (f) critical current of the electrolytes of interest at various temperatures.

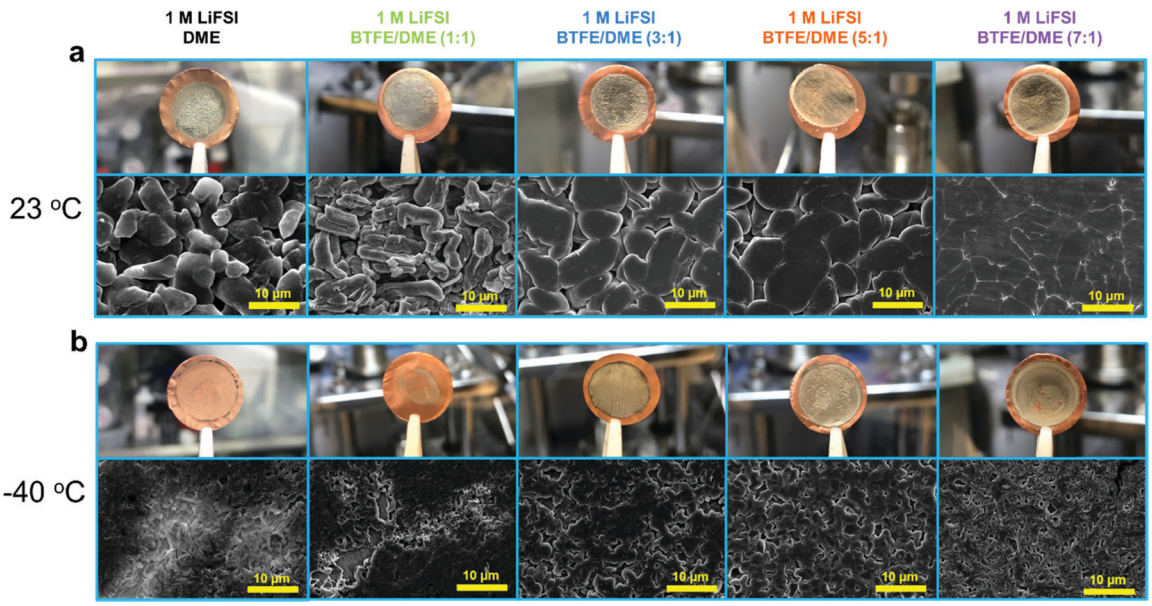


Fig. 4 Characterization of Li metal deposits in electrolytes of interest. Optical and SEM photographs of 5 mA h $cm^{-2}$ of Li metal deposited at (a) 23 °C and (b) −40 °C. All depositions were carried out at 0.5 mA $cm^{-2}$.

concentration. This may be a direct result of the increased electrochemical stability of the electrolyte associated with higher concentration, where salt driven passivation of the interphase is typically achieved due to the restriction of reactive solvent by the strongly coordinated $Li^+$.[25–29,33–35,37]

When carrying out the same deposition process at −40 °C we observed a distinct shift in both the macroscopic and microscopic structure, however. Similar to the previously presented data, we believe the origin of this behavior and its asymmetric temperature dependence across systems corresponds to the local concentration of each system and the coincident ion-pairing of their solvation shells. First, it was observed that the amount of Li plated on the Cu current collectors in 1 M LiFSI DME and 1 M LiFSI BTFE/DME (1 : 1) undergoes a severe reduction at −40 °C. This phenomenon has been observed in our previous work[23] and is believed to be a direct indication that these systems suffer from severe shorting at low temperature which renders Li plating unnecessary to balance the charge of the electrochemical circuit. Furthermore, bundles of nano-sized dendritic filaments were observed in the 1 M LiFSI DME sample (Fig. S7, ESI†), which may be directly responsible for the shorting behavior. On the other hand, homogenous Li deposition was achieved in 1 M LiFSI BTFE/DME 3 : 1, 5 : 1, and 7 : 1 systems, which agrees with the trends observed in the CE measurements at −40 °C and below. Notably, the optimum in terms of deposit size and uniformity at −40 °C was produced by 1 M LiFSI BTFE/DME (5 : 1) instead of the 7 : 1 solution, which may suggest that among systems of comparable charge-transfer kinetics the relatively poor ionic conductivity of the 7 : 1 electrolyte may be problematic. Despite this, the reduced Li deposition size produced by the 7 : 1 electrolyte at −40 °C did not result in a clear reduction in CE relative to the 3 : 1 and 5 : 1 electrolytes, which is likely related to the inherently lower reactivity of this heavily ion-paired system. We have also observed dendritic growth in the Li deposits produced by 1 M LiFSI BTFE/DME (1 : 1) at −20 °C, which coincides with a substantial decrease in CE despite the lack of soft-shorting phenomena (Fig. S8, ESI†). Such dendritic growth was also found to result in a significant increase in plated Li porosity, where 4 mA h $cm^{-2}$ of plated Li was found to exhibit thicknesses of 32.7, 25.3, 22.6, and 23.2 μm for 1 M LiFSI BTFE/DME (1 : 1), (3 : 1), (5 : 1), and (7 : 1), respectively (Fig. S9, ESI†).

As previously discussed, the charge-transfer barrier is thought to be the limiting factor at low temperatures. Such behavior and its temperature dependence is defined by the inner and outer-sphere reorganization energies (further discussed below), themselves defined by the solvation environment of $Li^+$ in solution.[22,38–42] To understand this microscopic solvation structure in the LHCE systems, we performed classical MD simulations. Here, ~500 total molecules were assembled in various ratios of $Li^+$, $FSI^-$, DME, and BTFE, depending on the electrolyte in question (Table S1, ESI†), and subjected to 25 ns of production dynamics after initial equilibration, from which the solvation data were extracted. A more detailed description of these simulations is provided in the ESI.† Representative snapshots from the MD simulations can be found in Fig. 5a, where it can be seen that

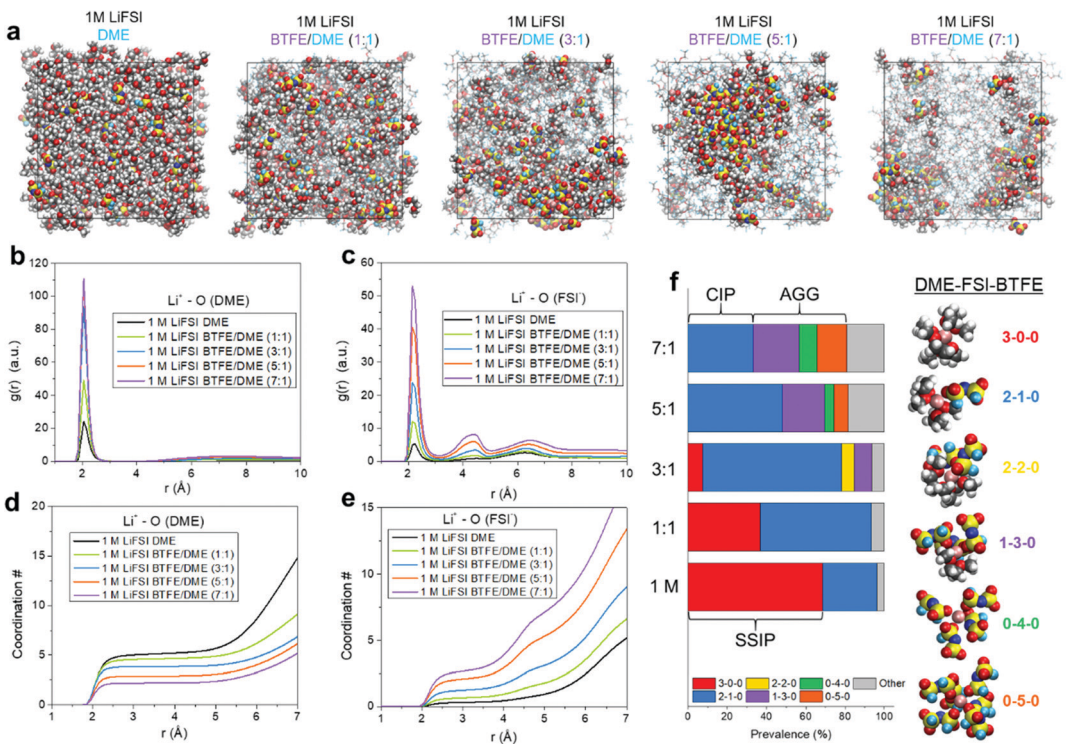


Fig. 5 Molecular dynamics analysis of electrolytes of interest. (a) Snapshots of MD simulations. Radial distribution functions of (b) DME and (c) $FSI^-$ oxygens with respect to $Li^+$. Coordination numbers of (d) DME and (e) $FSI^-$ oxygens with respect to $Li^+$. (f) Solvation structure distribution analysis of systems of interest and representative MD snapshot of each significant coordination environment.

 

the spatial distribution of the ions shift substantially as the concentration increases. At the highest DME/$Li^+$ ratio (9.6 : 1) found in 1 M LiFSI DME, the $Li^+$ ions are distributed homogenously in solution. However, at the higher local concentrations found in the 3 : 1 electrolyte and above, significant aggregation of solvating clusters composed of $Li^+$, $FSI^-$ and DME separated by regions of BTFE was found. This local aggregation effect is also observed in a previous *ab initio* MD work,[43] and partially accounts for the reduced ionic conductivity of the systems with high local concentrations. The stochastic trajectory of the $Li^+$ ion over the 25 ns is presented in Fig. S11 (ESI†) to visualize the effect of aggregation on ionic motion. We reason that this effect is a symptom of the disparate solvating power of DME and BTFE, where the $Li^+$ ion far prefers interaction with the former, forming ion-pairs as the amount of available DME decreases.[28]

To quantify the local environment around the $Li^+$ ion in solution, the radial distribution function (RDF) with respect to $Li^+$ was calculated. Fig. 5b and c shows the RDF due to the oxygens of DME and $FSI^-$ respectively, and the associated integrals (*i.e.* the coordination number) is shown in Fig. 5d and e. This analysis revealed that 1 M LiFSI in DME largely prefers a solvent-separated ion-pair structure (SSIP), in which the $Li^+$ is coordinated only by solvent in the first solvation shell. Our previous work has noted that the DME dominated SSIP solvation environment is correlated with poor low temperature performance.[23] However, with increasing local concentration (increased BTFE/DME ratio) the DME in the primary solvation shell was sequentially displaced by $FSI^-$ molecules, such that the average coordination of environments of the 1 M LiFSI DME and 7 : 1 electrolytes were calculated to be $Li^+(DME\text{-}O)_{5.0}(FSI\text{-}O)_{0.3}$ and $Li^+(DME\text{-}O)_{3.0}(FSI\text{-}O)_{2.5}$, respectively. BTFE was not found to solvate $Li^+$ in any statistically significant manner (Fig. S12, ESI†), which is also supported by the Raman spectra (Fig. 2d). It is noteworthy that there is generally a distinction made between different ion-paired states, where one coordinating $FSI^-$ per $Li^+$ is typically deemed a "contact-ion-pair" (CIP), while $FSI^-$ coordination numbers $> 1$ are denoted as an "aggregate" (AGG).[26] In this regard, the RDF data suggests that SSIP, CIP, and AGG structures dominate as the local concentrations increases.

Though the RDF data reveals the average solvation structure, in this case, they fail to properly describe the distribution of solvation states the $Li^+$ takes in each system. To explore this, 250 snapshots of each $Li^+$ and its local environment were extracted for each simulation (between 10 750 and 12 500 snapshots depending on the simulation) and tabulated (Supporting Information). In this analysis, we adopted the naming convention "*X*–*Y*–*Z*" to denote the number of DME (*X*), $FSI^-$ (*Y*), and BTFE (*Z*) found within the first solvation shell of Li (within 3 Å). It was found that the 1 M LiFSI DME electrolyte most prominently displayed a local environment of 3–0–0 (68.5%), with a lower prevalence of 2–1–0 (27.8%) which correspond to SSIP and contact-ion-pair (CIP) solvation environments, respectively. More moderate local concentrations (*e.g.*, 3 : 1) were found to be dominated by CIP, while the higher concentrations tended to prefer AGG states. Though the calculated $Li^+$ transference numbers indicate that the MD simulations may slightly exaggerate the ion-pairing character of these systems, this trend is maintained (Fig. S3, ESI†). Representative structures for each system are shown in Fig. 2f, and alternatively displayed in Fig. S12f (ESI†). Consistent with our previous work,[23] we now elaborate on how the CIP/aggregate dominated systems are advantageous at low temperatures.

It has been widely observed that charge transfer impedance at low temperatures overwhelms and thus dictates the performance of Li-based batteries at low temperatures, which we have recently hypothesized to be the cause of the dendritic growth and subsequent shorting of LMBs under such conditions.[2,22,23] The experimental and theoretical evidence presented in this work establishes a more robust correlation between ion-pairing and improved Li reversibility at low temperature. While this information is practically useful for low temperature electrolyte design, it is crucial to note that a causal string has not yet been identified. The temperature dependence of charge-transfer in Li-based batteries is a complicated topic that undoubtedly warrants further study, however there are a number of recent works that may provide additional insights into the phenomena observed here.

To gain further insights into the charge-transfer phenomena, we take a perspective based on Marcus Theory. This framework and its subsequent iterations are generally thought to be the most accurate model of electrochemical kinetics at the interphase, and have recently been demonstrated to accurately describe Li metal plating.[38–42,44] Perhaps the most relevant parameter to our work, which partially defines both the adiabaticity and energy of the transition state is the reorganization parameter $\lambda$, which generally consists of inner-sphere and outer-sphere components. The former describes the reorganization energy of the electronic structure and vibrational modes within the solvation sphere, while the latter describes the energetic cost of nuclear motion (*i.e.*, deformation) of the coordinating species. To interpret the results presented here, and in keeping with previous studies,[39–41] it is generally assumed that inner-sphere reorganization is largely temperature independent, whereas outer-sphere reorganization is significantly temperature dependent.

The effect of ion-pairing on these reorganization factors has been typically studied in a variety of electrochemical systems, where it has been suggested that increased pairing results in improved outer-sphere energetics.[45,46] In aprotic media, the formation of ion-pairs in the double layer has been proposed to allow the cation to approach the interphase at smaller distances than SSIP structures,[46] which preliminary quantum chemistry results indicate may be the case in this work, where $FSI^-$ removal was found to be unlikely when compared to DME removal (Fig. S13, ESI†). It is also worth noting that different degrees of ion pairing were found to display different behavior at said interphases, which may also describe the variance in performance between the 3 : 1, 5 : 1, and 7 : 1 electrolytes.[46] However, recent work from Boyle *et al.* indicates that these conclusions may not directly translate to improved Li metal kinetics at room temperature.[44] This work found that though

the interphasial impedance was substantially lowered by the introduction of ion-pairs, the reorganization parameter underwent little change. We hypothesize that this is a direct result of an increased contribution from $e^-$ transfer resistance (*i.e.* inner-sphere) to the total reorganization energy in ion-paired systems. Additionally, the presence of ion-pairing was also concluded to reduce the electronic coupling between the electrode and $Li^+$, which may be a direct result of increased binding energy between $Li^+$ and the anion (Fig. S13, ESI†). While this reduced coupling is broadly detrimental to charge-transfer, the nature of electronic phenomena suggests it has little influence on temperature dependent performance. Considering the temperature dependence of inner and outer-sphere reorganization, these results would predict that the increased ion pairing in our systems gives rise to similar behavior at room temperature, but leads to disparate scaling at low temperatures, consistent with our experimental findings. Further, our model is supported by the recent work from Wang *et al.*, which suggested that electrolytes dominated by $Li^+$/DME interactions have a particularly large entropy of $Li/Li^+$ exchange, which is incrementally reduced by the introduction of ion-pairing in solution.[32]

Though a definitive causal understanding of temperature dependent Li metal plating has not been reached, this work demonstrates that the introduction of ion-pairing in the electrolyte results in vastly improved Li metal cycling at low temperatures. To provide a more practical demonstration of these advantages, 2× excess Li||NMC 811 full cells were assembled and subjected to a variety of performance tests at room and low temperatures. The 1 M LiFSI DME and 1 M LiFSI BTFE/DME (1 : 1) systems were applied as SSIP-containing controls and compared to 1 M LiFSI BTFE/DME (5 : 1) due to its relative balance between low temperature CE, critical current, and oxidative stability (Fig. 6a and b). Though the systems exhibiting an SSIP structure are sub-optimal choices due to their reduced oxidative stability (Fig. 2c and Fig. S2, ESI†), such a comparison is necessary to examine the influence of solvation structure on low temperature energy retention and cyclability. These cells were assessed in two modes of operation: charging at room temperature followed by a low temperature discharge, and both charging and discharging at the temperature of interest. As shown in Fig. 6d and e, the cells employing 1 M LiFSI DME and 1 M LiFSI BTFE/DME (1 : 1) were found to output 195, 149, and 122 mA h $g^{-1}$ and 203, 163, and 154 mA h $g^{-1}$ (with respect to the cathode), respectfully when discharged at 23, −20, and −40 °C and after being charged at room temperature. The relative increase in low temperature discharge capacity between 1 M LiFSI DME and the 1 M LiFSI BTFE/DME (1 : 1) system is possibly due to the increased CIP

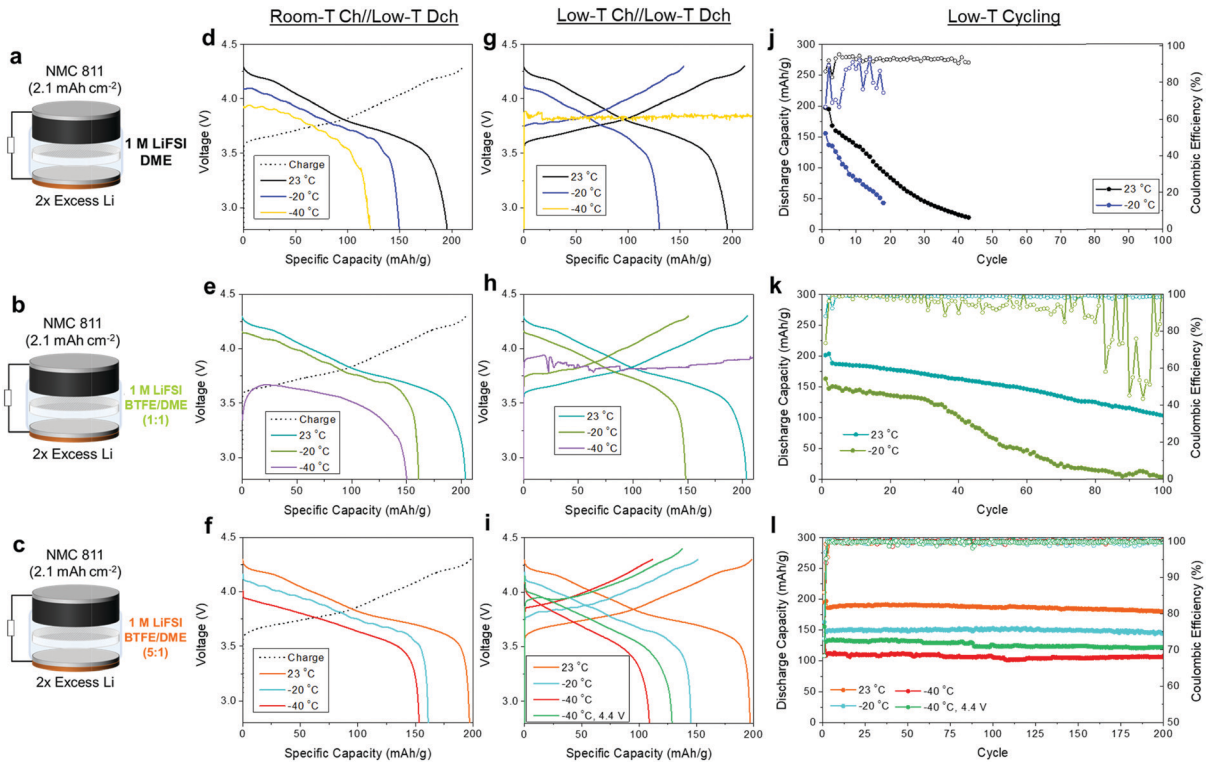


Fig. 6 2× Li||NMC 811 full cell operation at room and low temperature. Schematics of full cells employing (a) 1 M LiFSI DME, (b) 1 M LiFSI BTFE/DME (1 : 1), and (c) 1 M LiFSI BTFE/DME (5 : 1) under flooded electrolyte conditions. 0.1C rate discharge profiles of full cells charged at room temperature employing (d) 1 M LiFSI DME, (e) 1 M LiFSI BTFE/DME (1 : 1), and (f) 1 M LiFSI BTFE/DME (5 : 1). Cycle profiles of full cells charged and discharged at various temperatures employing (g) 1 M LiFSI DME, (h) 1 M LiFSI BTFE/DME (1 : 1), and (i) 1 M LiFSI BTFE/DME (5 : 1). All displayed voltage profiles represent the first available cycle post conditioning step. Cycling performance of full cells employing (j) 1 M LiFSI DME, (k) 1 M LiFSI BTFE/DME (1 : 1), and (l) 1 M LiFSI BTFE/DME (5 : 1). Room temperature cycling was carried out at C/3||C/3 rates after 2 cycles at C/10 and low temperature cycling was carried out at C/10||C/5 for charge||discharge, respectively. Full cells were charged once at room temperature before transferring to low temperature.

 

character in the 1 : 1 mixture. Conversely, the 1 M LiFSI BTFE/DME (5 : 1) full cells displayed 197, 161, and 153 mA h $g^{-1}$ under the same conditions, indicative of improved electrochemical kinetics over the controls despite significantly reduced bulk transport metrics (Fig. 6f). Note that this operation scheme does not involve Li plating at low temperature and thus shorting was intentionally avoided.

High performance retention in the 5 : 1 electrolyte was also observed when subject to both charge and discharge at reduced temperature, displaying discharge capacities of 145 and 109 mA h $g^{-1}$ at −20 and −40 °C, respectively (Fig. 6i). It is noteworthy that the ohmic polarization of discharge at −40 °C is slightly improved compared to that which was charged at room temperature (Fig. 6f), which may be due to the higher surface are of Li, or variance of the SEI formed at such temperatures.[9] Additionally, it was found that this output capacity could be increased to 129 mA h $g^{-1}$ by increasing the cutoff voltage from 4.3 V to 4.4 V at −40 °C, which may partially compensate for ohmic losses on the anode side at low temperature. This performance is not shared by the 1 M LiFSI DME and 1 M LiFSI BTFE/DME (1 : 1) electrolyte cells under the same conditions, which retained 130 and 147 mA h $g^{-1}$ when charged and discharged at −20 °C before undergoing complete soft shorting at −40 °C. As previously discussed, we attribute these results to the favorable temperature scaling of the charge-transfer process in ion-paired electrolytes, which is consistent with 3-electrode impedance studies, which show a substantially reduced barrier for the 5 : 1 electrolyte down to −40 °C for both the cathode and anode (Fig. S14, ESI†). These performance results are consistent with the critical current results, and demonstrates that electrolytes which exhibit SSIP structures are untenable for application in low temperature LMBs.

When subjected to cycling, the 1 M LiFSI DME full cells were found to be unable to retain meaningful capacity, retaining 136 and 80 mA h $g^{-1}$ after 10 cycles at 23 and −20 °C, respectively (Fig. 6j). This performance is likely a combined effect of the poor oxidative stability of the electrolyte, which may exacerbate transition metal dissolution on the cathode side, as well as the comparatively poor Li reversibility of the 1 M LiFSI DME system.[47] Full cells employing the 1 : 1 electrolyte retained 154 and 103 mA h $g^{-1}$ after 50 and 100 cycles at 23 °C, representing a substantial improvement over the 1 M LiFSI DME electrolyte, which may be partially due to the stability of the cathode electrolyte interphase (CEI) formed by BTFE (Fig. S15, ESI†). Hence, the 1 M LiFSI BTFE/DME (1 : 1) and provides a valid cycling baseline at ambient temperature to examine the effect of solvation structure on low temperature performance. As predicted by the previous trends (Fig. 3), the poor Li metal cycling efficiency of the 1 : 1 electrolyte at −20 °C (Fig. 3b) was found to severely limit performance, where the output capacity significantly decreased after 30 cycles, falling to 66 and 3.7 mA h $g^{-1}$ at the 50th and 100th cycle, respectively (Fig. 6k). On the other hand, the full cells employing 1 M LiFSI BTFE/DME (5 : 1) were found to retain stable performance over 200 cycles without undergoing a meaningful reduction in output capacity or coulombic efficiency that is generally associated with exhaustion of the Li metal anode reservoir (Fig. 6l).[30] The capacity retention of these cells after 100 cycles were found to be 187, 153, 108, and mA h $g^{-1}$ at 23, −20, −40 (4.3 V cutoff), and −40 °C (4.4 V cutoff). The improved performance of the 1 M LiFSI BTFE/DME (5 : 1) electrolyte is evidence that LMBs can be cycled at low temperature reversibly without the need for thermal management.

To supplement the performance assessment of coin cells employing the electrolytes of interest, scale-up projections were carried out to provide the expected energy density as a function of temperature and operating scheme. The projections were based on 5 Ah pouch cells at an N/P capacity ratio of 2 (2× excess Li) and a 3 g A $h^{-1}$ electrolyte loading, with the specific capacities and average voltages taken from the first cycle of the coin cell data (Fig. S16, ESI†). More details are available in the Supporting Information. At a cathode loading of 2 mA h $cm^{-2}$, these projections estimate that pouch cells employing 1 M LiFSI DME and charged at room temperature could achieve energy densities of 303, 237, and 192 W h $kg^{-1}$ whereas cells employing 1 M LiFSI BTFE/DME (1 : 1) project to produce 309, 247, and 213 W h $kg^{-1}$ at 23, −20, and −40 °C, respectively. Under the same conditions, the 1 M LiFSI BTFE/DME (5 : 1) is expected to achieve 307, 250, and 230 W h $kg^{-1}$. When both charged and discharged at the temperature of interest, the 1 M LiFSI DME energy densities are expected to fall to 207, and 0 W h $kg^{-1}$ (due to shorting) whereas 1 M LiFSI BTFE/DME (1 : 1) are expected to fall to 226, and 0 W h $kg^{-1}$ at −20 and −40 °C, respectively. Conversely, the 5 : 1 electrolyte is expected to output 224, 163, and 194 W h $kg^{-1}$ at −20, −40 (4.3 V cutoff), and −40 °C (4.4 V cutoff), respectively. Additionally, increasing the cathode loading to 3 mA h $cm^{-2}$ in the 5 : 1 electrolyte under the same conditions is expected to increase these values to 342, 249, 181, and 216 W h $kg^{-1}$ at 23, −20, −40 (4.3 V cutoff), and −40 °C (4.4 V cutoff), respectively. Preliminary results indicate this optimization may be possible (Fig. S17, ESI†), however the engineering of practical LMB pouch cells capable of low temperature cycling remains a difficult task. If such a battery were realized at scale, the NASA 20LuSTR program goals of a >250 W h $kg^{-1}$ secondary battery operating at <−40 °C for over 100 cycles would be within reach.[48] While the electrolytes investigated here provide a scientific comparison of the effects of ion-pairing on the temperature dependence of Li metal reversibility, it should be noted that electrolytes employing solvents of a lower $Li^+$ binding energy may improve the performance even further at low temperatures.

## Conclusions

A series of LHCE electrolytes composed of LiFSI, DME, and BFTE with varying local concentrations were designed and compared to probe the effect of ion-paring in the local solvation structure on the low temperature performance of Li metal plating and stripping. It was found that despite comparable room temperature performance, only systems with DME/$Li^+$ molecular ratios of 2.4 and below were capable of providing

reversible Li cycling at −20 °C and below. What's more, this performance trend was found to be in opposition to the ionic transport data, which seemed to indicate that systems of low local concentration were superior. Through MD analysis, it was found that this performance transition was coincident with a distinct shift in $Li^+$ solvation structure in which ion-pairing was a defining feature, and purely solvent dominated environments were due to the lack of available DME molecules. Though this evidence is still correlational in nature, previous reports indicate that ion-pairing may shift the balance of inner-sphere, which is thought to be temperature independent, and outer-sphere reorganization energies such that low-temperature performance is improved. Finally, 2× excess Li||NMC 811 full cells were assembled utilizing both electrolytes of high and low local concentrations to demonstrate the translation of these solvation effects during cell operation. Specifically, the cells employing electrolytes with significant ion-pairing nature were able to demonstrate 100 cycles of reversible performance with little capacity fade while retaining 63% of their room temperature energy. This work unambiguously demonstrates the positive effects of ion-paired solvation structures on the low temperature Li metal reversibility while providing a viable route to LMBs charged and discharged at low temperatures.

## Author contributions

J. H. conceived the original idea. P. L. and Z. C. directed the project. J. H., and K. K., carried out the experiments. Y. Y., Z. W., H. L., and M. L. assisted with characterization. T. A. P. directed the computational experiments. J.H. and A.C. conducted computational experiments. H. G. and G. C. assisted in experimental design and data processing. J. H., Z. C., P. L., and T. A. P. wrote the paper. All authors discussed the results and commented on the manuscript.

## Conflicts of interest

The authors declare no competing interests.

## Acknowledgements

This work was supported by NASA Space Technology Graduate Research Opportunity 80NSSC20K1174. Z. C. acknowledges the support by an Early Career Faculty grant from NASA's Space Technology Research Grants Program (ECF 80NSSC18K1512). The authors also acknowledge the use of facilities and instrumentation supported by NSF through the UC San Diego Materials Research Science and Engineering Center (UCSD MRSEC) DMR-2011924. Part of the work used the UCSD-MTI Battery Fabrication Facility and the UCSD-Arbin Battery Testing Facility. Electron microscopic characterization was performed at the San Diego Nanotechnology Infrastructure (SDNI) of UCSD, a member of the National Nanotechnology Coordinated Infrastructure, which is supported by the National Science Foundation (Grant ECCS-1542148). This work also used the Extreme Science and Engineering Discovery Environment (XSEDE)[49] on the Expanse supercomputer at the San Diego Supercomputing center, which is supported by National Science Foundation grant number ACI-1548562.

## References

1 A. Gupta and A. Manthiram, Designing Advanced Lithium-Based Batteries for Low-Temperature Conditions, *Adv. Energy Mater.*, 2020, **10**, 2001972.
2 S. S. Zhang, K. Xu and T. R. Jow, The Low Temperature Performance of Li-Ion Batteries, *J. Power Sources*, 2003, **115**(1), 137–140.
3 M. C. Smart, B. V. Ratnakumar, K. B. Chin and L. D. Whitcanack, Lithium-Ion Electrolytes Containing Ester Cosolvents for Improved Low Temperature Performance, *J. Electrochem. Soc.*, 2010, **157**(12), A1361–A1374.
4 Q. Li, S. Jiao, L. Luo, M. S. Ding, J. Zheng, S. S. Cartmell, C.-M. Wang, K. Xu, J.-G. Zhang and W. Xu, Wide-Temperature Electrolytes for Lithium-Ion Batteries, *ACS Appl. Mater. Interfaces*, 2017, **9**(22), 18826–18835.
5 M. C. Smart, B. V. Ratnakumar, R. C. Ewell, S. Surampudi, F. J. Puglia and R. Gitzendanner, The Use of Lithium-Ion Batteries for JPL's Mars Missions, *Electrochim. Acta*, 2018, **268**, 27–40.
6 J. Liu, Z. Bao, Y. Cui, E. J. Dufek, J. B. Goodenough, P. Khalifah, Q. Li, B. Y. Liaw, P. Liu, A. Manthiram, Y. S. Meng, V. R. Subramanian, M. F. Toney, V. V. Viswanathan, M. S. Whittingham, J. Xiao, W. Xu, J. Yang, X.-Q. Yang and J.-G. Zhang, Pathways for Practical High-Energy Long-Cycling Lithium Metal Batteries, *Nat. Energy*, 2019, **4**(3), 180–186.
7 W. Xu, J. Wang, F. Ding, X. Chen, E. Nasybulin, Y. Zhang and J.-G. Zhang, Lithium Metal Anodes for Rechargeable Batteries, *Energy Environ. Sci.*, 2014, **7**(2), 513–537.
8 S. Li, M. Jiang, Y. Xie, H. Xu, J. Jia and J. Li, Developing High-Performance Lithium Metal Anode in Liquid Electrolytes: Challenges and Progress, *Adv. Mater.*, 2018, **30**(17), 1706375.
9 A. C. Thenuwara, P. P. Shetty and M. T. McDowell, Distinct Nanoscale Interphases and Morphology of Lithium Metal Electrodes Operating at Low Temperatures, *Nano Lett.*, 2019, **19**(12), 8664–8672.
10 A. C. Thenuwara, P. P. Shetty, N. Kondekar, S. E. Sandoval, K. Cavallaro, R. May, C.-T. Yang, L. E. Marbella, Y. Qi and M. T. McDowell, Efficient Low-Temperature Cycling of Lithium Metal Anodes by Tailoring the Solid-Electrolyte Interphase, *ACS Energy Lett.*, 2020, **5**(7), 2411–2420.
11 X. Dong, Y. Lin, P. Li, Y. Ma, J. Huang, D. Bin, Y. Wang, Y. Qi and Y. Xia, High-Energy Rechargeable Metallic Lithium Battery at −70 °C Enabled by a Cosolvent Electrolyte, *Angew. Chem., Int. Ed.*, 2019, **58**(17), 5623–5627.
12 H. Cheng, Q. Sun, L. Li, Y. Zou, Y. Wang, T. Cai, F. Zhao, G. Liu, Z. Ma, W. Wahyudi, Q. Li and J. Ming, Emerging Era

 

of Electrolyte Solvation Structure and Interfacial Model in Batteries, *ACS Energy Lett.*, 2022, **7**(1), 490–513.

13 X.-K. Hou, S.-F. Li, W.-H. Li, H.-J. Liang, Z.-Y. Gu, X.-X. Luo and X.-L. Wu, Electrolyte Chemistry Towards Improved Cycling Stability in Na-Based Dual-Ion Batteries with High-Power/Energy Storage, *Batteries Supercaps*, 2021, **4**(10), 1647–1653.

14 H.-J. Liang, Z.-Y. Gu, X.-X. Zhao, J.-Z. Guo, J.-L. Yang, W.-H. Li, B. Li, Z.-M. Liu, W.-L. Li and X.-L. Wu, Ether-Based Electrolyte Chemistry Towards High-Voltage and Long-Life Na-Ion Full Batteries, *Angew. Chem., Int. Ed.*, 2021, **60**(51), 26837–26846.

15 C. S. Rustomji, Y. Yang, T. K. Kim, J. Mac, Y. J. Kim, E. Caldwell, H. Chung and Y. S. Meng, Liquefied Gas Electrolytes for Electrochemical Energy Storage Devices, *Science*, 2017, **356**(6345), eaal4263.

16 X. Fan, X. Ji, L. Chen, J. Chen, T. Deng, F. Han, J. Yue, N. Piao, R. Wang, X. Zhou, X. Xiao, L. Chen and C. Wang, All-Temperature Batteries Enabled by Fluorinated Electrolytes with Non-Polar Solvents, *Nat. Energy*, 2019, **4**(10), 882–890.

17 C.-Y. Wang, G. Zhang, S. Ge, T. Xu, Y. Ji, X.-G. Yang and Y. Leng, Lithium-Ion Battery Structure That Self-Heats at Low Temperatures, *Nature*, 2016, **529**(7587), 515–518.

18 Y. Ji and C. Y. Wang, Heating Strategies for Li-Ion Batteries Operated from Subzero Temperatures, *Electrochim. Acta*, 2013, **107**, 664–674.

19 X. Dong, Z. Guo, Z. Guo, Y. Wang and Y. Xia, Organic Batteries Operated at −70 °C, *Joule*, 2018, **2**(5), 902–913.

20 M. C. Smart, B. L. Lucht, S. Dalavi, F. C. Krause and B. V. Ratnakumar, The Effect of Additives upon the Performance of MCMB/$LiNi_xCo_{1-x}O_2$ Li-Ion Cells Containing Methyl Butyrate-Based Wide Operating Temperature Range Electrolytes, *J. Electrochem. Soc.*, 2012, **159**(6), A739–A751.

21 J. Zhang, J. Zhang, T. Liu, H. Wu, S. Tian, L. Zhou, B. Zhang and G. Cui, Towards Low-Temperature Lithium Batteries: Advances and Prospects of Unconventional Electrolytes, *Advanced Energy and Sustainability Research*, 2021, **2**(10), 2100039.

22 Q. Li, D. Lu, J. Zheng, S. Jiao, L. Luo, C.-M. Wang, K. Xu, J.-G. Zhang and W. Xu, $Li^+$ -Desolvation Dictating Lithium-Ion Battery's Low-Temperature Performances, *ACS Appl. Mater. Interfaces*, 2017, **9**(49), 42761–42768.

23 J. Holoubek, H. Liu, Z. Wu, Y. Yin, X. Xing, G. Cai, S. Yu, H. Zhou, T. A. Pascal, Z. Chen and P. Liu, Tailoring Electrolyte Solvation for Li Metal Batteries Cycled at Ultra-Low Temperature, *Nat. Energy*, 2021, **6**(3), 303–313.

24 Z. Wang, Z. Sun, Y. Shi, F. Qi, X. Gao, H. Yang, H.-M. Cheng and F. Li, Ion-Dipole Chemistry Drives Rapid Evolution of Li Ions Solvation Sheath in Low-Temperature Li Batteries, *Adv. Energy Mater.*, 2021, **11**(28), 2100935.

25 Y. Yamada, J. Wang, S. Ko, E. Watanabe and A. Yamada, Advances and Issues in Developing Salt-Concentrated Battery Electrolytes, *Nat. Energy*, 2019, **4**(4), 269–280.

26 J. Wang, Y. Yamada, K. Sodeyama, C. H. Chiang, Y. Tateyama and A. Yamada, Superconcentrated Electrolytes for a High-Voltage Lithium-Ion Battery, *Nat. Commun.*, 2016, **7**(1), 12032.

27 X. Fan, L. Chen, X. Ji, T. Deng, S. Hou, J. Chen, J. Zheng, F. Wang, J. Jiang, K. Xu and C. Wang, Highly Fluorinated Interphases Enable High-Voltage Li-Metal Batteries, *Chem*, 2018, **4**(1), 174–185.

28 S. Chen, J. Zheng, D. Mei, K. S. Han, M. H. Engelhard, W. Zhao, W. Xu, J. Liu and J.-G. Zhang, High-Voltage Lithium-Metal Batteries Enabled by Localized High-Concentration Electrolytes, *Adv. Mater.*, 2018, **30**(21), 1706102.

29 X. Ren, L. Zou, X. Cao, M. H. Engelhard, W. Liu, S. D. Burton, H. Lee, C. Niu, B. E. Matthews, Z. Zhu, C. Wang, B. W. Arey, J. Xiao, J. Liu, J.-G. Zhang and W. Xu, Enabling High-Voltage Lithium-Metal Batteries under Practical Conditions, *Joule*, 2019, **3**(7), 1662–1676.

30 C. Niu, H. Lee, S. Chen, Q. Li, J. Du, W. Xu, J.-G. Zhang, M. S. Whittingham, J. Xiao and J. Liu, High-Energy Lithium Metal Pouch Cells with Limited Anode Swelling and Long Stable Cycles, *Nat. Energy*, 2019, **4**(7), 551–559.

31 J. Wang, W. Huang, A. Pei, Y. Li, F. Shi, X. Yu and Y. Cui, Improving Cyclability of Li Metal Batteries at Elevated Temperatures and Its Origin Revealed by Cryo-Electron Microscopy, *Nat. Energy*, 2019, **4**(8), 664–670.

32 H. Wang, S. C. Kim, T. Rojas, Y. Zhu, Y. Li, L. Ma, K. Xu, A. T. Ngo and Y. Cui, Correlating Li-Ion Solvation Structures and Electrode Potential Temperature Coefficients, *J. Am. Chem. Soc.*, 2021, **143**(5), 2264–2271.

33 K. Ueno, K. Yoshida, M. Tsuchiya, N. Tachikawa, K. Dokko and M. Watanabe, Glyme–Lithium Salt Equimolar Molten Mixtures: Concentrated Solutions or Solvate Ionic Liquids?, *J. Phys. Chem. B*, 2012, **116**(36), 11323–11331.

34 X. Ren, L. Zou, S. Jiao, D. Mei, M. H. Engelhard, Q. Li, H. Lee, C. Niu, B. D. Adams, C. Wang, J. Liu, J.-G. Zhang and W. Xu, High-Concentration Ether Electrolytes for Stable High-Voltage Lithium Metal Batteries, *ACS Energy Lett.*, 2019, **4**(4), 896–902.

35 E. R. Fadel, F. Faglioni, G. Samsonidze, N. Molinari, B. V. Merinov, W. A. G. Iii, J. C. Grossman, J. P. Mailoa and B. Kozinsky, Role of Solvent-Anion Charge Transfer in Oxidative Degradation of Battery Electrolytes, *Nat. Commun.*, 2019, **10**(1), 3360.

36 B. D. Adams, J. Zheng, X. Ren, W. Xu and J.-G. Zhang, Accurate Determination of Coulombic Efficiency for Lithium Metal Anodes and Lithium Metal Batteries, *Adv. Energy Mater.*, 2018, **8**(7), 1702097.

37 J. Qian, W. A. Henderson, W. Xu, P. Bhattacharya, M. Engelhard, O. Borodin and J.-G. Zhang, High Rate and Stable Cycling of Lithium Metal Anode, *Nat. Commun.*, 2015, **6**, 6362.

38 R. A. Marcus, On the Theory of Electron-Transfer Reactions. VI. Unified Treatment for Homogeneous and Electrode Reactions, *J. Chem. Phys.*, 1965, **43**(2), 679–701.

39 M. D. Newton and N. Sutin, Electron Transfer Reactions in Condensed Phases, *Annu. Rev. Phys. Chem.*, 1984, **35**(1), 437–480.

40 C. E. D. Chidsey, Free Energy and Temperature Dependence of Electron Transfer at the Metal–Electrolyte Interface, *Science*, 1991, **251**(4996), 919–922.
41 D. L. Derr and C. M. Elliott, Temperature Dependence of the Outer-Sphere Reorganization Energy, *J. Phys. Chem. A*, 1999, **103**(39), 7888–7893.
42 R. Nazmutdinov, P. Quaino, E. Colombo, E. Santos and W. Schmickler, A Model for the Effect of Ion Pairing on an Outer Sphere Electron Transfer, *Phys. Chem. Chem. Phys.*, 2020, **22**(25), 13923–13929.
43 S. Perez Beltran, X. Cao, J.-G. Zhang and P. B. Balbuena, Localized High Concentration Electrolytes for High Voltage Lithium–Metal Batteries: Correlation between the Electrolyte Composition and Its Reductive/Oxidative Stability, *Chem. Mater.*, 2020, **32**(14), 5973–5984.
44 D. T. Boyle, X. Kong, A. Pei, P. E. Rudnicki, F. Shi, W. Huang, Z. Bao, J. Qin and Y. Cui, Transient Voltammetry with Ultramicroelectrodes Reveals the Electron Transfer Kinetics of Lithium Metal Anodes, *ACS Energy Lett.*, 2020, **5**(3), 701–709.
45 B. Huang, K. H. Myint, Y. Wang, Y. Zhang, R. R. Rao, J. Sun, S. Muy, Y. Katayama, J. Corchado Garcia, D. Fraggedakis, J. C. Grossman, M. Z. Bazant, K. Xu, A. P. Willard and Y. Shao-Horn, Cation-Dependent Interfacial Structures and Kinetics for Outer-Sphere Electron-Transfer Reactions, *J. Phys. Chem. C*, 2021, **125**(8), 4397–4411.
46 A. Baskin, J. W. Lawson and D. Prendergast, Anion-Assisted Delivery of Multivalent Cations to Inert Electrodes, *J. Phys. Chem. Lett.*, 2021, **12**(18), 4347–4356.
47 H. Y. Asl and A. Manthiram, Reining in Dissolved Transition-Metal Ions, *Science*, 2020, **369**(6500), 140–141.
48 National Aeronautics and Space Administration. Space Technology Research Grants, Lunar Surface Technology Research Opportunities Appendix. 2020.
49 J. Towns, T. Cockerill, M. Dahan, I. Foster, K. Gaither, A. Grimshaw, V. Hazlewood, S. Lathrop, D. Lifka, G. D. Peterson, R. Roskies, J. R. Scott and N. Wilkins-Diehr, XSEDE: Accelerating Scientific Discovery, *Comput. Sci. Eng.*, 2014, **16**(5), 62–74.

 